

Low-energy enhancement in the magnetic dipole γ -ray strength functions of heavy nuclei

P. Fanto* and Y. Alhassid[†]

Center for Theoretical Physics, Sloane Physics Laboratory, Yale University, New Haven, Connecticut 06511, USA



(Received 26 December 2021; revised 26 June 2023; accepted 2 February 2024; published 7 March 2024)

A low-energy enhancement (LEE), which was observed experimentally in the γ -ray strength function (γ SF) describing the decay of compound nuclei, would have profound effects on r -process nucleosynthesis if it persists in heavy neutron-rich nuclei. The LEE was shown to be a feature of the magnetic dipole ($M1$) strength function in configuration-interaction shell-model calculations in medium-mass nuclei. However, its existence in heavy open-shell nuclei remains an open question. Here, using a combination of many-body methods, we identify a LEE in the $M1$ γ SFs of heavy samarium nuclei. In particular, we use the static-path plus random-phase approximation (SPA+RPA), which includes static and small-amplitude quantal fluctuations beyond the mean field. Using the SPA+RPA strength as a prior, we apply the maximum-entropy method to obtain finite-temperature $M1$ γ SFs from exact imaginary-time response functions calculated with the shell-model Monte Carlo method. We find that the slope of the LEE in samarium isotopes is roughly independent of the average initial energy over a wide range below the neutron separation energy. As the neutron number increases, strength transfers to a low-energy excitation, which we interpret as the scissors mode built on top of excited states.

DOI: [10.1103/PhysRevC.109.L031302](https://doi.org/10.1103/PhysRevC.109.L031302)

Introduction. The γ -ray strength function (γ SF) [1] is an important input to the Hauser-Feshbach theory of compound-nucleus reactions [2] and has a significant effect on r -process nucleosynthesis [3]. In particular, the magnetic dipole ($M1$) γ SF in heavy nuclei exhibits interesting phenomenology, characterized by a spin-flip resonance and a scissors mode [4,5]. The inclusion of the latter in Hauser-Feshbach calculations improves predictions of neutron radiative capture rates [6].

In recent years, a low-energy enhancement (LEE)—an up-bend structure at low γ -ray energies—has been observed experimentally in the γ SFs for decay in several midmass nuclei [7–9] and a few rare-earth nuclei [10–12]. If it persists in heavy neutron-rich nuclei, the LEE is likely to have profound effects on r -process nucleosynthesis since it would enhance significantly the radiative neutron capture cross sections of nuclei near the neutron drip line [13]. Experiments indicate that the LEE is of dipole nature [14], and configuration-interaction (CI) shell-model studies of medium-mass nuclei have attributed the LEE to the $M1$ γ SF [15–20]. A LEE was also observed in CI shell-model calculations of the $M1$ strength function of $A \approx 130$ nuclei [21]. However, conventional CI shell-model diagonalization methods become intractable in heavier nuclei due to the combinatorial increase of the many-particle model space with the numbers of valence nucleons and/or single-particle orbitals. Consequently, there has been no theoretical investigation of the persistence of the LEE in heavy open-shell nuclei.

While most theoretical studies have focused on the strength function built on the ground state, finite-temperature

methods enable the study of γ SFs built on excited states. The finite-temperature quasiparticle random-phase approximation (QRPA) has been applied to calculate finite-temperature γ SFs [22–25], and the zero-temperature QRPA with empirical corrections has also been applied to γ SF calculations [26,27]. However, the QRPA has limitations in that it only includes small-amplitude quantal fluctuations around the mean-field configuration, and its finite-temperature version has been mostly limited to spherical nuclei.

The shell-model Monte Carlo (SMMC) method [28–31] enables exact calculations (to within statistical errors) of finite-temperature observables within the CI shell-model framework; see Ref. [32] for a recent review. However, the SMMC cannot calculate the finite-temperature γ SF directly, but only its Laplace transform, the imaginary-time response function. The γ SF is then the inverse Laplace transform of the imaginary-time response function, which requires the analytic continuation to real time and is numerically an ill-posed inverse problem. The standard method to carry out this analytic continuation is the maximum-entropy method (MEM) [33–35], but its success depends crucially on the choice a good prior strength function.

Here we use the static-path plus random-phase approximation (SPA+RPA) [36–38] to construct a prior strength function. The SPA+RPA includes large-amplitude static fluctuations [39] and small-amplitude time-dependent quantal fluctuations beyond the mean field and was recently successfully applied to study nuclear state densities of heavy nuclei [40]. The SPA+RPA restores the full rotational symmetry that is broken in the mean-field approximation in deformed nuclei, and was shown to describe correctly the rotational enhancement of state densities in deformed nuclei. In the SPA+RPA, we can calculate real-time response functions directly, and

*paulfanto11@gmail.com; yoram.alhassid@yale.edu

therefore an analytic continuation is not required to obtain its corresponding strength function.

In this work we apply the MEM to calculate the finite-temperature $M1$ γ SF from the SMMC imaginary-time response functions using the SPA+RPA strength as a prior in a chain of heavy even-mass samarium isotopes $^{148-154}\text{Sm}$. Furthermore, we extract the deexcitation strength functions from these finite-temperature strength functions and find an enhancement at low γ -ray energies that is present over a broad range of temperatures (i.e., average initial excitation energies), which we interpret as the LEE. A LEE was identified experimentally in the total γ SF of several odd-mass samarium isotopes [10,11]. The deexcitation γ SF was measured in the even-mass samarium isotope ^{148}Sm [41] but a LEE was not observed.

In the finite-temperature $M1$ γ SFs, we also observe a transfer of strength from the low-energy peak to a somewhat higher-energy excitation as the neutron number increases and the isotopes become more deformed. We interpret this higher-lying excitation as the scissors mode [4,5] built on top of excited states [42].

SPA+RPA γ SF. The γ SF at temperature T for an electromagnetic transition operator, which is a spherical tensor \mathcal{O}_λ of rank λ , is defined by

$$S_{\mathcal{O}_\lambda}(T; \omega) = \sum_{\substack{\alpha_f J_f \\ \alpha_i J_i}} \frac{e^{-\beta E_{\alpha_f J_f}}}{Z} |(\alpha_f J_f || \hat{\mathcal{O}}_\lambda || \alpha_i J_i)|^2 \times \delta(\omega - E_{\alpha_f J_f} + E_{\alpha_i J_i}), \quad (1)$$

where (αJ) label CI shell-model eigenstates with energy and spin $(E_{\alpha J}, J)$, and $Z = \sum_{\alpha J} (2J+1)e^{-\beta E_{\alpha J}}$ is the canonical partition function. Given a shell-model Hamiltonian with the two-body interaction expressed in the separable form $\hat{H}_2 = -(1/2) \sum_{\alpha} v_{\alpha} \hat{Q}_{\alpha}^2$, we apply the adiabatic approximation of Ref. [38] to evaluate Eq. (1) in the SPA+RPA

$$S_{\mathcal{O}_\lambda}(T; \omega) \approx \frac{\int d\sigma M(\sigma) Z_{\eta}(\sigma) C_{\eta}(\sigma) S_{\mathcal{O}_\lambda, \eta}(T, \sigma; \omega)}{\int d\sigma M(\sigma) Z_{\eta}(\sigma) C_{\eta}(\sigma)}, \quad (2)$$

where σ are static auxiliary fields and $M(\sigma)$ is a measure function [40]. $Z_{\eta}(\sigma) = \text{Tr}[\hat{P}_{\eta} e^{-\beta(\hat{h}_{\sigma} - \sum_{\lambda=p,n} \mu_{\lambda} \hat{N}_{\lambda})}]$ is the number-parity projected one-body partition function, where $\hat{h}_{\sigma} = \hat{H}_1 - \sum_{\alpha} v_{\alpha} \sigma_{\alpha} \hat{Q}_{\alpha}$ is a one-body Hamiltonian, and $P_{\eta} = (1 + \eta e^{i\pi \hat{N}})/2$ is the number-parity projection with $\eta = +1(-1)$ for even (odd) number parity. $C_{\eta}(\sigma)$ is the RPA correction factor that accounts for the Gaussian integral over small amplitude time-dependent auxiliary-field fluctuations [36,37,40,43,44]. This correction factor is given by (see Eq. (8) of Ref. [40])

$$C_{\eta}(\sigma) = \frac{\prod_{k>l} \frac{1}{\tilde{E}_k - \tilde{E}_l} \sinh(\beta(\tilde{E}_k - \tilde{E}_l)/2)}{\prod_{v>0} \frac{1}{\tilde{\Omega}_v} \sinh(\beta\tilde{\Omega}_v/2)}, \quad (3)$$

where \tilde{E}_k are the generalized quasiparticle energies of \hat{h}_{σ} and $\pm\tilde{\Omega}_v$ are the eigenvalues of the σ -dependent RPA matrix

$$\mathcal{M}_{k_l, k'l'}^{\eta} = (\tilde{E}_k - \tilde{E}_l) \delta_{kk'} \delta_{ll'} - \frac{1}{2} (\tilde{f}_l^{\eta} - \tilde{f}_k^{\eta}) \sum_{\alpha} \mathcal{Q}_{\alpha, kl} \mathcal{Q}_{\alpha, l'k'}. \quad (4)$$

Here \tilde{f}_k^{η} are the number-parity-projected generalized thermal quasiparticle occupation numbers; see Ref. [40] for further details.

The σ -dependent strength function $S_{\mathcal{O}_\lambda, \eta}(T, \sigma; \omega)$ in Eq. (2) is given by [38]

$$S_{\mathcal{O}_\lambda, \eta}(T, \sigma; \omega) = S_{\mathcal{O}_\lambda, \eta}^{(0)}(T, \sigma) \delta(\omega) - \lim_{\epsilon \rightarrow 0^+} \frac{\text{Im} \Pi_{\mathcal{O}_\lambda, \eta}(T, \sigma; \omega + i\epsilon)}{\pi(1 - e^{-\beta\omega})}, \quad (5)$$

where

$$\Pi_{\mathcal{O}_\lambda, \eta}(T, \sigma; \omega + i\epsilon) = \sum_{\mu} \sum_{kl, k'l'} \sum_v \frac{1}{2} \mathcal{O}_{\lambda\mu, kl}^* \mathcal{M}_{kl, v}^{\eta} \mathcal{M}_{v, k'l'}^{\eta, -1} \times (\tilde{f}_l^{\eta} - \tilde{f}_{k'}^{\eta}) \mathcal{O}_{\lambda\mu, k'l'} \frac{1}{\omega - \tilde{\Omega}_v + i\epsilon}. \quad (6)$$

In Eq. (6), v ranges over the eigenbasis of the RPA matrix \mathcal{M} and μ denotes the components of \mathcal{O}_λ . The second term on the right-hand side of Eq. (5) corresponds to the finite-temperature QRPA strength function around the mean-field configuration defined by the static auxiliary fields σ [45,46]. For each such static configuration we explicitly exclude all the spurious zero-energy modes associated with broken symmetries. The first term on the right-hand side accounts for the strength in the $\omega \rightarrow 0$ limit, for which we use the SPA result [38]

$$S_{\mathcal{O}_\lambda, \eta}^{(0)}(T, \sigma) = \frac{1}{2} \sum_{\mu} \sum_{\substack{kl, k'l' \\ E_k = E_l}} \mathcal{O}_{\lambda\mu, kl}^* \mathcal{O}_{\lambda\mu, k'l'} \langle a_k^{\dagger} a_l a_k^{\dagger} a_l \rangle_{\sigma, \eta}, \quad (7)$$

where a_k, a_k^{\dagger} annihilate and create quasiparticles in the eigenbasis of \hat{h}_{σ} .

We express Eq. (2) in terms of the weight function $\mathcal{W}_{\eta}(\sigma) = M(\sigma) Z_{\eta}(\sigma)$

$$S_{\mathcal{O}_\lambda}(T; \omega) = \frac{\int d\sigma \mathcal{W}_{\eta}(\sigma) C_{\eta}(\sigma) S_{\mathcal{O}_\lambda, \eta}(T, \sigma; \omega)}{\int d\sigma \mathcal{W}_{\eta}(\sigma) C_{\eta}(\sigma)}. \quad (8)$$

Following Ref. [40], we apply the Metropolis-Hastings algorithm to draw uncorrelated sample configurations σ_k from the weight function \mathcal{W}_{η} and evaluate Eq. (8) by taking an average over these sample configurations,

We also calculate the finite-temperature γ SF in the static-path approximation (SPA), which neglects the quantal fluctuations entirely. In this case, the RPA correction factor $C_{\eta} = 1$, and the σ -dependent γ SF in Eq. (5) is given by its mean-field expression.

Maximum-entropy method. We improve our SPA+RPA calculations of the finite-temperature γ SF by combining these results with exact SMMC calculations of the imaginary-time response function $R_{\mathcal{O}_\lambda}(T; \tau)$ through the maximum-entropy method (MEM) [34]. $R_{\mathcal{O}_\lambda}(T; \tau)$ is the Laplace transform of the finite-temperature γ SF. The γ SF satisfies $S_{\mathcal{O}_\lambda}(T; -\omega) = e^{-\beta\omega} S_{\mathcal{O}_\lambda}(T; \omega)$ and the Laplace transform can be rewritten as

$$R_{\mathcal{O}_\lambda}(T; \tau) = \int_0^{\infty} d\omega K(\tau, \omega) S_{\mathcal{O}_\lambda}(T; \omega), \quad (9)$$

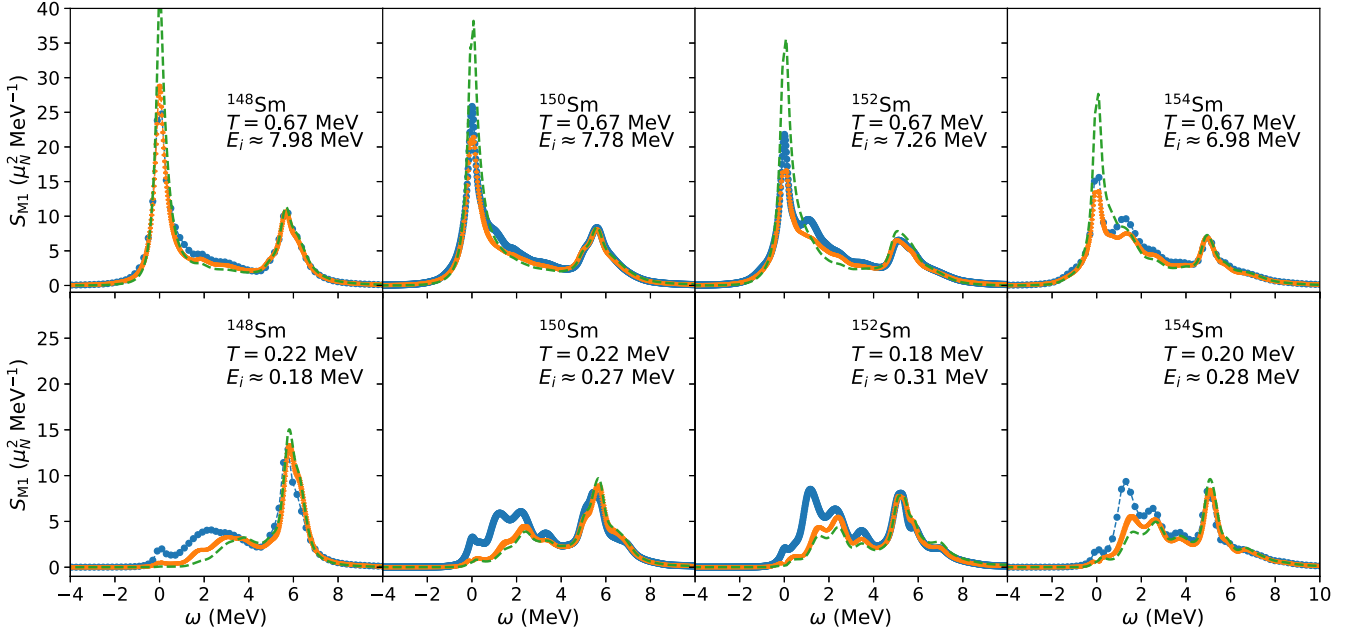


FIG. 1. The finite-temperature $M1$ γ SF as a function the transition energy ω for the even-mass samarium isotopes $^{148-154}\text{Sm}$. The MEM results (green dashed lines) are compared with the SPA+RPA results (orange dots) and SPA results (blue circles). The top row shows temperatures near the neutron separation energies in each of the isotopes, while the bottom row shows low temperatures close to the ground state.

where $K(\tau, \omega) = e^{-\tau\omega} + e^{-(\beta-\tau)\omega}$ is a symmetrized kernel that decays exponentially with ω . The MEM selects the γ SF that maximizes the objective function [34]

$$\mathcal{Q}(S_{\mathcal{O}_\lambda}; \alpha) = \alpha S - \frac{1}{2}\chi^2. \quad (10)$$

In Eq. (10), the χ^2 function is given by

$$\chi^2 = (\bar{R}_{\mathcal{O}_\lambda} - R_{\mathcal{O}_\lambda})^T \mathcal{C}^{-1} (\bar{R}_{\mathcal{O}_\lambda} - R_{\mathcal{O}_\lambda}), \quad (11)$$

where \bar{R} is the SMMC response function in imaginary time and \mathcal{C} is its covariance matrix. S is the entropy function

$$S = - \int d\omega (S_{\mathcal{O}_\lambda}(T; \omega) - S_{\mathcal{O}_\lambda}^{\text{prior}}(T; \omega) - S_{\mathcal{O}_\lambda}(T; \omega) \ln [S_{\mathcal{O}_\lambda}(T; \omega) / S_{\mathcal{O}_\lambda}^{\text{prior}}(T; \omega)]), \quad (12)$$

where $S_{\mathcal{O}_\lambda}^{\text{prior}}$ is a suitably chosen prior for the γ SF.

In this work, we apply Bryan's method [47], in which the MEM strength function is given by

$$S_{\mathcal{O}_\lambda}^{\text{MEM}} = \int d\alpha S_{\mathcal{O}_\lambda}^\alpha \mathcal{P}(\alpha | \bar{G}_{\mathcal{O}_\lambda}, \mathcal{C}, S_{\mathcal{O}_\lambda}^{\text{prior}}), \quad (13)$$

where $S_{\mathcal{O}_\lambda}^\alpha$ maximizes the objective function (10) for a given α , and the probability function $\mathcal{P}(\alpha | \bar{G}_{\mathcal{O}_\lambda}, \mathcal{C}, S_{\mathcal{O}_\lambda}^{\text{prior}})$ is given in Ref. [34].

In the SMMC method, the imaginary-time response function of \mathcal{O}_λ is expressed as [30,32]

$$R_{\mathcal{O}_\lambda}(T; \tau) = \frac{\int D[\sigma] G_\sigma \text{Tr} \hat{U}_\sigma \langle \mathcal{O}_\lambda(\tau) \cdot \mathcal{O}_\lambda \rangle_\sigma}{\int D[\sigma] G_\sigma \text{Tr} \hat{U}_\sigma}, \quad (14)$$

where $\mathcal{O}_\lambda(\tau) = \hat{U}_\sigma^{-1}(\tau, 0) \mathcal{O}_\lambda \hat{U}_\sigma(\tau, 0)$ with $\hat{U}_\sigma(\tau, 0)$ being the propagator for a system of noninteracting nucleons moving in

external time-dependent auxiliary fields σ , G_σ is a Gaussian weight, and the expectation value $\langle \dots \rangle_\sigma$ is taken with respect to the propagator $\hat{U}_\sigma \equiv \hat{U}_\sigma(\beta, 0)$. We sample auxiliary-field configurations according to the weight function $\mathcal{W}_\sigma^{\text{SMMC}} = G_\sigma |\text{Tr} \hat{U}_\sigma|$ and average over these samples to determine the response function estimate and covariance matrix. In contrast to the SPA+RPA, the SMMC includes all fluctuations of the time-dependent auxiliary fields σ . We will discuss our SPA+RPA method and MEM approach in more detail elsewhere.

Application to lanthanide nuclei. We calculated finite-temperature $M1$ γ SFs in a chain of even-mass samarium isotopes $^{148-154}\text{Sm}$ with the SPA+RPA and used the MEM to refine these strength functions. We used the single-particle model space and Hamiltonian of Ref. [40] with a pairing plus quadrupole two-body interaction. The $M1$ operator has the form

$$\hat{O}_{M1} = \sqrt{\frac{3}{4\pi}} \frac{\mu_N}{\hbar c} (g_l \mathbf{l} + g_s \mathbf{s}), \quad (15)$$

where \mathbf{l} and \mathbf{s} are the orbital and spin angular momentum operators, respectively. In our calculations, we used the free-nucleon g factors $g_{l,p} = 1$, $g_{l,n} = 0$, $g_{s,p} = 5.5857$, and $g_{s,n} = -3.8263$.

In Fig. 1, we show the finite-temperature $M1$ γ SF. We compare the MEM γ SF results (green dashed lines) with the SPA+RPA results (orange dots) and SPA results (blue circles). The top row in Fig. 1 shows temperatures at which the average initial energy in each isotope is near the neutron separation energy, while the bottom row shows low temperatures at which the isotopes are essentially in their ground states. Positive values of ω correspond to the absorption of γ rays.

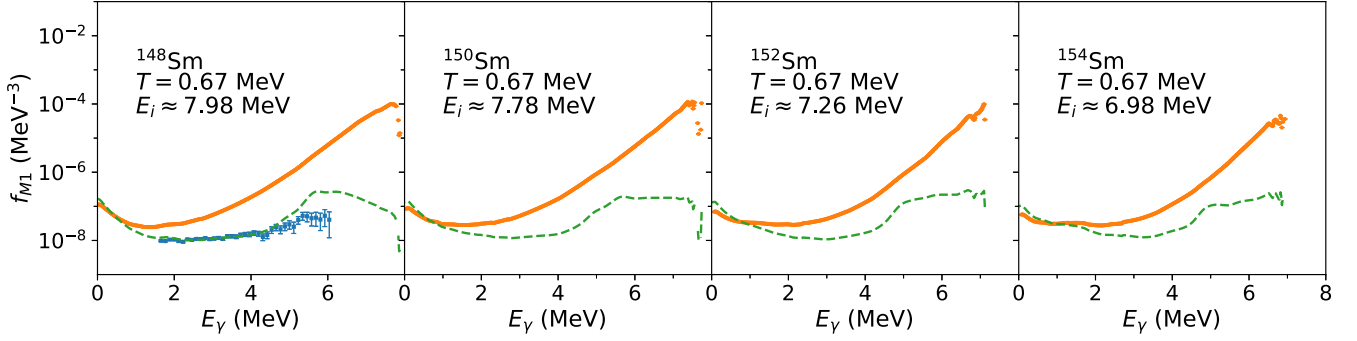


FIG. 2. The deexcitation strength function f_{M1} as a function of emitted γ -ray energy E_{γ} for the even-mass samarium isotopes $^{148-154}\text{Sm}$ at an average initial energy near their neutron separation energy. The MEM results (green dashed lines) are compared with the SPA+RPA results (orange dots). We observe the LEE in all four isotopes. For ^{148}Sm , we also show the experimental total deexcitation γ SF (blue solid squares) from Ref. [41].

The reliability of the MEM depends on a good choice for the prior strength function. In Fig. 1 of the Supplemental Material [48] we show the $M1$ imaginary-time response functions for the SPA and the SPA+RPA in comparison with the exact SMMC response function (which essentially coincides with the response function of the MEM strength function). We observe that the SPA+RPA response function is close to the exact SMMC response function. This indicates that the SPA+RPA strength function is a good prior and thus our MEM results are reliable.

In Fig. 1, we replaced the δ functions in the σ -dependent strength functions (5) with Lorentzians of fixed width $\epsilon = 0.2$ MeV. This width is comparable to the bin width in final energy used in previous CI shell-model studies [15,17–20].

For transitions starting near the neutron separation energy (top row of Fig. 1), the main effect of the MEM is to increase the height of the peak at $\omega \approx 0$. As shown in Fig. 2 below, this $\omega \approx 0$ peak corresponds to the LEE. At higher ω values, the MEM is in excellent agreement with the SPA+RPA result, which was used as a prior. As the neutron number increases, the strength of this $\omega \approx 0$ peak is reduced, and a small excitation around $\omega \approx 2$ MeV emerges in the γ SF. The location of this $\omega \approx 2$ MeV peak corresponds roughly to the location of the scissors mode observed in transitions from the ground state [4,5], and we therefore tentatively interpret it as the scissors mode built on excited states [42]. Our result that some of the LEE strength transfers to the scissors mode in deformed nuclei is consistent with the results of Ref. [18] in open-shell iron isotopes. Similarly, a reduction of the LEE peak at $E_{\gamma} \rightarrow 0$ with increasing number of active protons or number of active neutron holes in nuclei with $A \approx 130$ was observed in Ref. [21]. We also note in the top row of Fig. 1 an excitation at $\omega \approx 6$ MeV with a strength that is roughly independent of neutron number. We note that the main low-energy structures (including the LEE) in the magnetic dipole strength function originate in the SPA (blue circles in Fig. 1), namely from the large static fluctuations of the mean field and that the QRPA alone is not sufficient to reproduce the LEE.

In the γ SF from the ground state shown in the bottom row of Fig. 1, we observe no zero- ω peak. Instead, as neutron number increases, strength transfers from an excitation at

$\omega \approx 6$ MeV, which we interpret to be the spin-flip mode, to a multihumped low-energy excitation at $\omega \approx 1-3$ MeV. This is roughly consistent with the appearance of the scissors mode with increasing deformation in heavy even-mass nuclei [5].

To investigate the LEE, we calculate the deexcitation $M1$ strength function f_{M1} as a function of the γ -ray energy from the finite-temperature γ SF. We estimate f_{M1} for an initial excitation energy E_i and an emitted γ -ray energy E_{γ} using

$$f_{M1}(E_i, E_{\gamma}) \approx \frac{1}{3} a \frac{\tilde{\rho}(E_i)}{\tilde{\rho}(E_i - E_{\gamma})} S_{M1}(T; \omega = -E_{\gamma}), \quad (16)$$

where $a = \frac{16\pi}{9(\hbar c)^3}$, T is the temperature describing an average excitation energy of E_i and $\tilde{\rho}(E_x)$ is the total level density. The latter is calculated from the total SMMC state density plus the spin-cutoff model. The factor of $1/3$ in Eq. (16) takes into account approximately the 3 allowed values of the final spin for a given initial spin [49]. As the LEE is a feature of compound-nucleus decay, we focus on downward transitions. In Fig. 2, we show the calculated f_{M1} versus the emitted γ -ray energy E_{γ} for average initial energies E_i near the neutron separation energy. In the MEM results (green dashed lines), we observe a LEE structure below $E_{\gamma} \approx 2$ MeV in each of the isotopes. This LEE is also present in the SPA+RPA results (orange dots) but is not as pronounced. We note that the response function is not sensitive to the strength function at high values of ω because of the exponential suppression in the Laplace transform (9). On the other hand, the low- ω results for the MEM strength function (for which the zero- ω peak is observed) are expected to be reliable and thus our MEM description of the LEE is likely to be accurate.

In the left panel of Fig. 2 we also included the experimental total deexcitation γ SF measured in Ref. [41] for ^{148}Sm (blue solid squares). We note that the experimental γ SF includes contributions from both $E1$ and $M1$, and a detailed comparison with the experiment requires the calculation of the $E1$ γ SF. Furthermore, since we work in a truncated shell-model space, the free-nucleons g factors used in our calculations can generally have renormalized values that might impact the calculated $M1$ strength function.

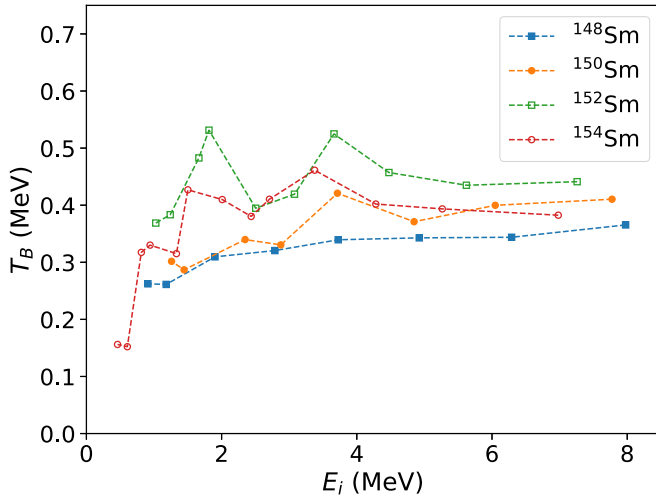


FIG. 3. The T_B parameter of the exponential form Ce^{-E_γ/T_B} fit to the f_{M1} results from the MEM at low E_γ for various average initial energies E_i . Results are shown for the even-mass samarium isotopes $^{148-154}\text{Sm}$.

The experimental γ SF of ^{148}Sm in Fig. 2 does not show a LEE but the lowest measured γ -ray energy is ≈ 1.65 MeV and our calculations indicate that it is necessary to go to lower energies to observe the LEE. In our calculations, we find the extrapolated LEE peak for ^{148}Sm at $E_\gamma \rightarrow 0$ to be $f_{M1} \approx 1.66 \times 10^{-7}$ MeV $^{-3}$. This value is comparable to the LEE peak observed experimentally [11] in the neighboring odd-mass nucleus ^{149}Sm with an extrapolated value for the peak of $\approx 1.3 \times 10^{-7}$ MeV $^{-3}$; see Fig. 5(d) of Ref. [11]. In Ref. [12], a LEE was observed in several neodymium isotopes with a peak of $\approx 1.05 \times 10^{-7}$ MeV $^{-3}$ in the spherical even mass ^{144}Nd (see Table IV in that reference).

Following Refs. [15,17], we fit an exponential form Ce^{-E_γ/T_B} to f_{M1} at low E_γ for various temperatures, each of which corresponds to an average initial energy E_i for the transition. We find that this exponential form provides a good description of the LEE structure. In Fig. 3, we show the fitted values of T_B for $^{148-154}\text{Sm}$ as a function of E_i . We find that the T_B values in each isotope remain roughly constant over a

wide range of E_i values. This independence of the slope of the LEE as a function of the initial energy is consistent with conventional CI shell-model results in smaller model spaces [17]. The T_B values for the isotopes are similar on average but are somewhat larger in the more deformed isotopes $^{152,154}\text{Sm}$, indicating that the LEE has a gentler slope in these isotopes. This is consistent with CI shell-model results in open-shell iron nuclei [18].

Conclusions. In this work, we applied the SPA+RPA to calculate finite-temperature $M1$ γ SFs in a chain of even-mass samarium isotopes $^{148-154}\text{Sm}$ within the CI shell-model framework. We also applied the MEM to derive the $M1$ γ SFs from the exact SMMC imaginary-time response functions using our SPA+RPA results as the prior strength. We calculated the deexcitation $M1$ strength function f_{M1} as a function of the γ -ray decay energy for the even-mass samarium isotopes $^{148-154}\text{Sm}$ and found a LEE structure. To our knowledge, this is the first theoretical description of a LEE in the $M1$ γ SF of heavy nuclei using the CI shell-model framework in very large model spaces for which conventional diagonalization methods are prohibited. We showed that the LEE is roughly independent of the average initial energy, in agreement with previous results in medium-mass nuclei. If a LEE also exists in heavy nuclei near the neutron drip line, it is expected to enhance the radiative neutron capture cross sections, and thus alter considerably r -process nucleosynthesis. We also observed the emergence of a structure consistent with the scissors mode both near the neutron separation energy and near the ground state as the neutron number increases. Finally, the methods we applied here are not specific to atomic nuclei, but are generally applicable to the calculation of strength functions in strongly interacting many-body quantum systems.

Acknowledgments. This work was supported in part by the U.S. DOE Grant No. DE-SC0019521, and by the U.S. DOE NNSA Stewardship Science Graduate Fellowship under cooperative Agreement No. NA-0003960. The calculations used resources of the National Energy Research Scientific Computing Center (NERSC), a U.S. Department of Energy Office of Science User Facility operated under Contract No. DE-AC02-05CH11231. We thank the Yale Center for Research Computing for guidance and use of the research computing infrastructure.

- [1] G. A. Bartholomew, E. D. Earle, A. J. Ferguson, J. W. Knowles, and M. A. Lone, in *Advances in Nuclear Physics*, edited by M. Baranger and E. Vogt (Springer, Boston, 1973).
- [2] A. J. Koning and D. Rochman, *Nucl. Data Sheets* **113**, 2841 (2012).
- [3] M. Mumpower, R. Surman, G. C. McLaughlin, and A. Aprahamian, *Prog. Part. Nucl. Phys.* **86**, 86 (2016).
- [4] D. Bohle, A. Richter, W. Steffen, A. E. L. Dieperink, N. Lo Iudice, F. Palumbo, and O. Scholten, *Phys. Lett. B* **137**, 27 (1984).
- [5] K. Heyde, P. von Neumann-Cosel, and A. Richter, *Rev. Mod. Phys.* **82**, 2365 (2010).
- [6] M. R. Mumpower, T. Kawano, J. L. Ullmann, M. Krlicka, and T. M. Sprouse, *Phys. Rev. C* **96**, 024612 (2017).
- [7] A. Voinov, E. Algin, U. Agvaanluvsan, T. Belgya, R. Chankova, M. Guttormsen, G. E. Mitchell, J. Rekstad, A. Schiller, and S. Siem, *Phys. Rev. Lett.* **93**, 142504 (2004).
- [8] A. C. Larsen, N. Blasi, A. Bracco, F. Camera, T. K. Eriksen, A. Gørgen, M. Guttormsen, T. W. Hagen, S. Leoni, B. Million, H. T. Nyhus, T. Renstrøm, S. J. Rose, I. E. Ruud, S. Siem, T. Tornyi, G. M. Tveten, A. V. Voinov, and M. Wiedeking, *Phys. Rev. Lett.* **111**, 242504 (2013).
- [9] A. C. Larsen, J. E. Midtbø, M. Guttormsen, T. Renstrøm, S. N. Liddick, A. Spyrou, S. Karampagia, B. A. Brown, O. Achakovskiy, S. Kamerdzhiev, D. L. Bleuel, A. Couture, L. C. Campo, B. P. Crider, A. C. Dombos, R. Lewis, S. Mosby, F. Naqvi, G. Perdikakis, C. J. Prokop *et al.*, *Phys. Rev. C* **97**, 054329 (2018).

- [10] A. Simon, M. Guttormsen, A. C. Larsen, C. W. Beausang, P. Humby, J. T. Harke, R. J. Casperson, R. O. Hughes, T. J. Ross, J. M. Allmond, R. Chyzh, M. Dag, J. Koglin, E. McCleskey, M. McCleskey, S. Ota, and A. Saastamoinen, *Phys. Rev. C* **93**, 034303 (2016).
- [11] F. Naqvi, A. Simon, M. Guttormsen, R. Schwengner, S. Frauendorf, C. S. Reingold, J. T. Harke, N. Cooper, R. O. Hughes, S. Ota, and A. Saastamoinen, *Phys. Rev. C* **99**, 054331 (2019).
- [12] M. Guttormsen, K. O. Ay, M. Ozgur, E. Algin, A. C. Larsen, F. L. Bello Garrote *et al.*, *Phys. Rev. C* **106**, 034314 (2022).
- [13] A. C. Larsen and S. Goriely, *Phys. Rev. C* **82**, 014318 (2010).
- [14] M. D. Jones, A. O. Macchiavelli, M. Wiedeking, L. A. Bernstein, H. L. Crawford, C. M. Campbell, R. M. Clark, M. Cromaz, P. Fallon, I. Y. Lee *et al.*, *Phys. Rev. C* **97**, 024327 (2018).
- [15] R. Schwengner, S. Frauendorf, and A. C. Larsen, *Phys. Rev. Lett.* **111**, 232504 (2013).
- [16] B. A. Brown and A. C. Larsen, *Phys. Rev. Lett.* **113**, 252502 (2014).
- [17] S. Karampagia, B. A. Brown, and V. Zelevinsky, *Phys. Rev. C* **95**, 024322 (2017).
- [18] R. Schwengner, S. Frauendorf, and B. A. Brown, *Phys. Rev. Lett.* **118**, 092502 (2017).
- [19] K. Sieja, *Phys. Rev. Lett.* **119**, 052502 (2017).
- [20] J. E. Midtbø, A. C. Larsen, T. Renstrøm, F. L. Bello Garrote, and E. Lima, *Phys. Rev. C* **98**, 064321 (2018).
- [21] K. Sieja, *Phys. Rev. C* **98**, 064312 (2018).
- [22] E. Litvinova and N. Belov, *Phys. Rev. C* **88**, 031302(R) (2013).
- [23] E. Litvinova and H. Wibowo, *Phys. Rev. Lett.* **121**, 082501 (2018).
- [24] H. Wibowo and E. Litvinova, *Phys. Rev. C* **100**, 024307 (2019).
- [25] E. Yüksel, N. Paar, G. Colò, E. Khan, and Y. F. Niu, *Phys. Rev. C* **101**, 044305 (2020).
- [26] M. Martini, S. Péru, S. Hilaire, S. Goriely, and F. Lechaftois, *Phys. Rev. C* **94**, 014304 (2016).
- [27] S. Goriely, S. Hilaire, S. Péru, and K. Sieja, *Phys. Rev. C* **98**, 014327 (2018).
- [28] C. W. Johnson, S. E. Koonin, G. H. Lang, and W. E. Ormand, *Phys. Rev. Lett.* **69**, 3157 (1992).
- [29] Y. Alhassid, D. J. Dean, S. E. Koonin, G. Lang, and W. E. Ormand, *Phys. Rev. Lett.* **72**, 613 (1994).
- [30] S. E. Koonin, D. J. Dean, and K. Langanke, *Phys. Rep.* **278**, 1 (1997).
- [31] Y. Alhassid, L. Fang, and H. Nakada, *Phys. Rev. Lett.* **101**, 082501 (2008).
- [32] Y. Alhassid, in *Emergent Phenomena in Atomic Nuclei from Large-Scale Modeling: A Symmetry-Guided Perspective*, edited by K. D. Launey (World Scientific, Singapore, 2017), pp. 267–298.
- [33] J. E. Gubernatis, M. Jarrell, R. N. Silver, and D. S. Sivia, *Phys. Rev. B* **44**, 6011 (1991).
- [34] M. Jarrell and J. E. Gubernatis, *Phys. Rep.* **269**, 133 (1996).
- [35] J. Gubernatis, N. Kawashima, and P. Werner, *Quantum Monte Carlo Methods: Algorithms for Lattice Models* (Cambridge University Press, Cambridge, 2016).
- [36] G. Puddu, P. F. Bortignon, and R. A. Broglia, *Ann. Phys. (NY)* **206**, 409 (1991).
- [37] H. Attias and Y. Alhassid, *Nucl. Phys. A* **625**, 565 (1997).
- [38] R. Rossignoli and P. Ring, *Nucl. Phys. A* **633**, 613 (1998).
- [39] B. Lauritzen, P. Arve, and G. F. Bertsch, *Phys. Rev. Lett.* **61**, 2835 (1988).
- [40] P. Fanto and Y. Alhassid, *Phys. Rev. C* **103**, 064310 (2021).
- [41] S. Siem, M. Guttormsen, K. Ingeberg, E. Melby, J. Rekstad, A. Schiller, and A. Voinov, *Phys. Rev. C* **65**, 044318 (2002).
- [42] M. Krtička and F. Bečvář, *Int. J. Mod. Phys. E* **20**, 488 (2011).
- [43] R. Rossignoli, N. Canosa, and P. Ring, *Phys. Rev. Lett.* **80**, 1853 (1998).
- [44] K. N. Nesterov and Y. Alhassid, *Phys. Rev. B* **87**, 014515 (2013).
- [45] H. M. Somermann, *Ann. Phys. (NY)* **151**, 163 (1983).
- [46] P. Ring, L. M. Robledo, J. L. Egido, and M. Faber, *Nucl. Phys. A* **419**, 261 (1984).
- [47] R. K. Bryan, *Eur. Biophys. J.* **18**, 165 (1990).
- [48] See Supplemental Material at <http://link.aps.org/supplemental/10.1103/PhysRevC.109.L031302> for further discussions of the imaginary-time response functions, as well as the data files and computer codes required to reproduce the figures.
- [49] D. DeMartini (private communication).